# MSEC2024-123878

# INVESTIGATION OF MATERIAL TRASPORT THROUGH TRIPLY PERIODIC MINIMAL SURFACE (TPMS) BONE SCAFFOLDS USING COMPUTATIONAL FLUID DYNAMICS (CFD)

#### **Brandon Coburn**

Department of Mechanical Engineering Marshall University Huntington, WV 25755, USA

#### **ABSTRACT**

Cell-laden, scaffold-based tissue engineering methods have been successfully utilized for the treatment of bone fractures and diseases, caused by factors such as trauma, tumors, congenital anomalies, and aging. In such methods, the rate of scaffold biodegradation, transport of nutrients and growth factors, as well as removal of cell metabolic wastes at the site of injury are critical fluid-dynamics factors, affecting cell proliferation and ultimately tissue regeneration. Therefore, there is a critical need to identify the underlying material transport mechanisms and factors associated with cell-seeded, scaffold-based bone tissue engineering.

The overarching goal of this study is to contribute to patient-specific, clinical treatment of bone pathology. The overall objective of the work is to establish computational fluid dynamics (CFD) models to identify: (i) the consequential mechanisms behind internal and external material transport through/over porous bone scaffolds and (ii) optimal triply periodic minimal surface (TPMS) scaffold designs toward cell-laden bone fracture treatment.

In this study, 10 internal-flow and 10 external-flow CFD models were established using ANSYS, correspondingly based on 10 single-unit TPMS bone scaffold designs, where the geometry of each design was parametrically created using Rhinoceros 3D software. The influence of several design parameters, such as surface representation iteration, merged toggle iso value, and wall thickness, on geometry accuracy as well as computational time, was investigated in order to obtain computationally efficient and accurate CFD models. The fluid properties (such as density and dynamic viscosity) as well as the boundary conditions (such as no-slip condition, inlet flow velocity, and pressure outlet) of the CFD models were set based on clinical/research values reported in the literature as well as according to the fundamentals of internal/external Newtonian

\* Contact author. Tel.: +1(315)395-4598; fax: +1(304)696-5454; e-mail address: <a href="mailto:salary@marshall.edu">salary@marshall.edu</a>.

## Roozbeh "Ross" Salary\*

Department of Mechanical Engineering Department of Biomedical Engineering Marshall University Huntington, WV 25755, USA

flow modeling. Several fluid characteristics, including flow velocity, flow pressure, and wall shear stress, were analyzed to observe material transport internally through and externally over the TPMS scaffold designs.

Regarding the internal flow CFD modeling, it was observed that "P.W. Hybrid" (i.e., Design #7) had the highest-pressure output, with "Neovius" (i.e., Design #1) following second to it. These two designs have a relatively flatter surface area. In addition, "Schwarz P" (i.e., Design #2) was the lowest pressure output of all 10 TPMS designs. "Neovius" and "Schwarz P" had the highest and lowest values of wall shear stress. Besides, the velocity streamlines analysis showed an increase in velocity along the curved sections of the scaffolds' geometry.

Regarding the external flow CFD modeling, it was observed that "Neovius" yielded the highest-pressure output within the inlet section, which contains the area of the highest-pressure location. Furthermore, "Diamond" (i.e., Design #8) displayed having the highest values of wall shear stress due to the results of fluid interaction that accrues with complex curved structures. Also, when we look at designs like "Schwarz G", the depiction of turbulent motion can be seen along the internal curved sections of the structure. As the external velocity streamlines decrease within the inner channels of the designs, this will lead to an increased pressure buildup due to the intrinsic interactions between the fluid with the walls.

Overall, the outcomes of this study pave the way for optimal design and fabrication of complex, bone-like tissues with desired material transport properties for cell-laden, scaffold-based treatment of bone fractures.

#### **KEYWORDS**

Computational Fluid Dynamics; Biomanufacturing; Triply Periodic Minimal Surfaces (TPMS); Bone Tissue Engineering.

## 1. INTRODUCTION

## 1.1. Goal and Objectives

Bone tissue engineering is an emerging field of regenerative medicine, using the principles of tissue engineering, stem cell biology, and biomedical engineering to fabricate functional tissue implants that can be inserted within a patient to repair or replace damaged/missing bone [1].

The motivation for this study is to observe the fluid flow dynamics within a porous scaffold, which will aid in understanding complex geometry structures with fluid interaction. Fluid transport is crucial in material interaction and cell proliferation to develop bone scaffolds. The characteristics of permeability help in bone growth, but the induction of fluid flow wall shear stress (WSS) characteristics affects the biological development of the scaffold. For WSS, the fluid flow can hinder or improve the growth of the cell. A high WSS can eliminate cellar development and vice versa for a lower WSS. Thus, the objective of this study is to use computational fluid dynamics (CFD) to analyze fluid flow through the scaffolds' internal/external geometry structure. A wide range of properties, such as pressure, velocity streamlines, and WSS, will be evaluated within this study. The aim is to explore how a fluid flow will pass through and over the pores of a scaffold and how it will interact with the geometry of the scaffold. This will give insight into how biological fluids interact within scaffold pores and microstructures, allowing for more efficient design and additive fabrication of scaffolds.

## 1.2. Identified Gaps in the Literature

A review of literature reveals that many research studies have examined porosity variations [2-4] and a small collection of TPMS structures using fluid dynamics to develop bone tissue scaffolds. There is a need for identification and characterization of a wider range of bone-like scaffolds with optimal properties for bone tissue engineering.

It was observed that Primitive structure had a relatively simple structure, allowing for easier design and characterization of flow properties, and good compressibility and permeability in the structure [5, 6]. Gyroid structure had self-supported features along with excellent mechanical properties [7]. In addition, Gyroid shows an excellent complex internal structure, aiding in fluid properties [8], along with adequate permeability and fluid tortuosity. Furthermore, the highest permeability can be seen at a porosity of 80%, which will aid in cellular growth [6, 9].

It was also reported that investigating geometrical parameters on WSS and permeability would be inevitable for scaffold design toward bone regeneration [10]. Body-centered cubic (BCC) scaffolds are also being used for their open-cell structure capabilities [8]. Schwartz diamond design shows good cellular growth due to high permeability, along with fluid tortuosity that aids in cell-scaffold interaction [9].

Studies have shown that TPMS scaffolds are more permeable than lattice scaffolds, overall. An example of this design is Schoen I-WP [11], which has satisfactory WSS and permeability [12].

Choosing scaffolds with high porosity and pore size is important to improve bone growth and ensure scaffold strength [13]. Schwarz designs have desirable bone scaffold characteristics due to their high surface area to volume ratio [14].

TPMS architecture has been shown to have good porous structures for interconnected pores, along with improved mechanical and physiological properties. In addition, some studies show that they can be optimal bone implants for regenerative medicine [15, 16]. Thus, TPMS designs have received more attraction for their excellent performance compared to lattice scaffolds [17].

However, the knowledge gap presented here requires a more comprehensive selection of the TPMS structure for bone scaffold fabrication. Many of the scaffolds presented in the literature for bone tissue engineering were simply chosen based on their prior mechanical performance, while an in-depth analysis and understanding of the complex dynamics of fluid flow-porosity interactions would be critical for optimal bone tissue regeneration. This gap is addressed in this study by analyzing the fluid dynamics of a broad range of critical TPMS structures.

This will aid in selecting an optimal design for 3D fabrication utilizing additive manufacturing methods [18]. Thus, this study aims to fill this knowledge gap by observing a comprehensive collection of ten TPMS structures as a collective whole to study the fluid properties with a uniform porosity to capture the true essence of its fluid behavior.

The TPMS structures can be seen in Figure 1, which is further delineated in Sec. 2.2.1. Also, this study covers the analysis of internal flow, focusing on the fluid properties of pressure contour, wall shear stress (WSS), and velocity streamline, which can be seen in Sec. 3 to understand how the TPMS structures' internal flow behavior will respawn. In addition, another knowledge gap is satisfied with the analysis of external flow evaluated to observe how environmental fluid behavior will affect the TPMS scaffold toward identification of optimal designs, as detailed in Sec. 3.2.

# 2. MATERIAL AND METHODS

#### 2.1. Materials

The material and methods section will detail what development method was used for producing the CFD TPMS Scaffold Design, along with meshing, applied governing equation, fluid properties, and boundary conditions used within the simulation. In addition, the numerical solution will discuss the scheme and method used within the ANSYS simulation.

# 2.2. Computational Fluid Dynamics (CFD) 2.2.1. Scaffold Design

A total of 10 TPMS scaffolds were designed using Rhion 7 with the Grasshopper extension. The designs can be seen in Figure 1, and the equation can be denoted by Table 1. The Millipede and Weaverbird programs were used to develop an algorithm to construct the TPMS design. Millipede and Weaverbird programs can visualize parametric equations into 3D rendering in a mesh structure.

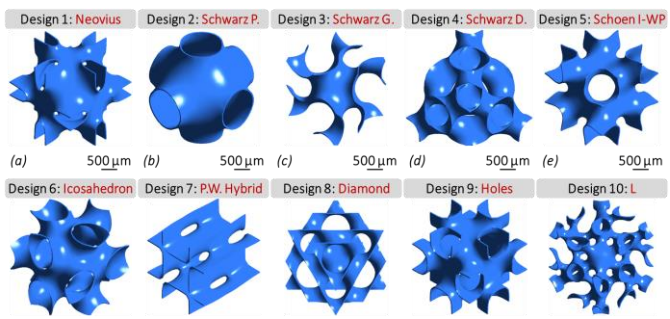


**Figure 1:** TPMS DESIGNS (IN ORDER OF DESIGN 1-10) DEVELOPED IN THIS STUDY FOR FABRICATION OF BONE SCAFFOLDS HAVING COMPLEX, POROUS INTERNAL MICROSTRUCTURES.

**Table 1:** PARAMETRIC EQUATIONS OF TPMS DESIGN 1 - 10.

Equations	TPMS Design
$3(\cos(x) + \cos(y) + \cos(z)) + 4(\cos(x)\cos(y)\cos(x))$	(1)
$-(\cos(x) + \cos(y) + \cos(z))$	(2)
$\sin(x)\cos(y) + \sin(z)\cos(x) + \sin(y)\cos(z)$	(3)
$\cos(x)\cos(y)\cos(z) - \sin(x)\sin(y)\sin(z)$	(4)
$2(\cos(x)\cos(y) + \cos(y)\cos(z) + \cos(z)\cos(x)) - (\cos(2x) + \cos(2y) + \cos(2z)$	(5)
$\cos\left(x + \frac{1+\sqrt{5}}{2y}\right) + \cos\left(x - \frac{1+\sqrt{5}}{2y}\right) + \cos\left(y + \frac{1+\sqrt{5}}{2z}\right) + \cos\left(y - \frac{1+\sqrt{5}}{2z}\right) + \cos\left(z + \frac{1+\sqrt{5}}{2x}\right) + \cos\left(z - \frac{1+\sqrt{5}}{2x}\right)$	(6)
$10(\cos(x)\cos(y)) + \cos(y)\cos(z) + \cos(z)\cos(x) \\ -0.01(\cos(x)\cos(y)\cos(z)$	(7)
$\sin(x)\sin(y)\sin(z) + \sin(x)\cos(y)\cos(z) + \cos(x)\sin(y)\cos(z) + \cos(x)\cos(y)\sin(z)$	(8)
$\cos(x) + \cos(y) + \cos(z) + 4\cos(x)\cos(y)\cos(z)$	(9)
$\frac{1}{2}\sin(2x)\cos(y)\sin(z) + \sin(2y)\cos(z)\sin(x) + \sin(2z)\cos(x)\sin(y) - \frac{1}{2}\cos(2x)\cos(2y) + \cos(2y)\cos(2z) + \cos(2z)\cos(2x)$	(10)

The parameter can be denoted for these designs within Table 2. All designs have the dimensions of a cube with a width, length, and height of 3 mm, respectively. The Step parameter is the iteration for the model generation. The Merged Toggle represents a collection of Boolean (True/False) values, along with IsoValue, representing a collection of double-precision floating point values. The ArrBox (x, y, z) Count supports constructing multiple units and attaching them into a cube to form a single structure. In addition, the level parameters control the number of subdivision iterations for each face on the designed model. The WBThickness controls the wall thickness of the model structure. In addition, design models 5, 9, and 10 have their step blocks changed to 16 to improve the simulation accuracy.

**Table 2:** TPMS DESIGN PARAMETERS WITHIN RHINO 7. NOTE THAT DESIGNS 5, 9, AND 10 HAVE A STEP VALUE OF 16.000.

Parameter	Values
Model Dimensions	3x3x3 mm (Cubic)
Step	18.710
Merged Toggle	True
IsoValue	-0.269
ArrBox(x, y, z) Count	1
Level	3
WBThickness Distance	0.042 mm

After rendering the TPMS design, they are exported into a file form of .3dm (Rhino 7 3D Models files), respectively. The design will be imported within Fluid Flow (Fluent with Fluent Meshing) ANSYS 2023 R2. Once the design is entirely imported, the conversion from facets to a solid will be done by the built-in function from SpaceClaim ANSYS. An encloser box is then built around the design geometry, having it placed within the center of the encloser box.

#### 2.2.2. Meshing

In the internal and external flow analysis, the 3D geometry is defined as watertight for fluid flow. Furthermore, these parameters can be denoted in Table 3 and Table 4. For internal flow, the model's geometry wall distance is set to 0.2 m uniformly from the inlet outlet and wall. As for the external flow geometry wall distance, the inlet and wall are set to 2 m, and the outlet distance is 5 m away for the model. The distance of 5 m is done to capture any development wake regions within the analysis. The local surface meshing sizes for both internal and external are 0.01, 0.001, and 0.0001 m, respectively, to the inlet, outlet, wall, domain, and scaffold model. In addition, for the surface and volume mesh, the growth is set to 1.2 m with a minimum surface size of 1.00E-05 m and a maximum surface size of 0.01 m.

Polyhedral was the meshing portion used to fill the cell volume elements. Furthermore, the solution residual sensitivity of the analysis is set at a convergence of 1.0E-06.

In addition, the Fill Type used for volume meshing is Uniform and Smoothing Transition. For the internal flow analysis, Designs 1, 9, and 10 used Smoothing Transition, with the rest using Uniform. As for the external flow analysis, only Design 1 used Smoothing Transition, and the rest used Uniform. Designs 9 and 10 did not need the Smoothing Transition because of the enlarged enclosure box around the design geometry. Furthermore, the Uniform's function is that each layer's thickness remains the same throughout the volume mesh.

Along with the direction vector at each node, it maintains uniformity. In addition, it can easily be maintained for flat or lightly curved surfaces [19]. As for the Smoothing Transition boundary layer, mesh thickness and first layer height vary along the surface depending on the local surface mesh size, resulting in a smooth transition on the model.

**Table 3:** NUMBER OF ELEMENTS IN EACH CFD DESIGN MODEL. THE MINIMUM ORTHOGONAL QUALITY IS AT 0.2 MESHING METRICS SPECTRUM.

External Cell Volume Elements	Internal Cell Volume Elements	Design Models
277566	257064	(1)
110624	102928	(2)
164854	151406	(3)
168451	154217	(4)
183322	165557	(5)
205754	190276	(6)
204218	189620	(7)
199373	186856	(8)
305409	285650	(9)
462513	446121	(10)

**Table 4:** CFD MESHING PARAMETERS FOR DESIGN 1 – 10 FOR INTERNAL AND EXTERNAL FLOW ANALYSIS

Parameter	Value
Internal Geometry Wall Distance from Model	0.2 (m)
External Geometry Wall Distance from Model (Inlet and Wall)	2 (m)
External Geometry Wall Distance from Model (Outlet)	5 (m)
Local Surface Meshing Sizing (Inlet, Outlet, and Wall)	0.01 (m)
Local Surface Meshing Sizing (Domain)	0.001 (m)
Local Surface Meshing Sizing (Model)	0.0001 (m)
Surface and Volume Growth Rate	1.2 (m)
Surface Mesh Minimum Size	1.00E-05 (m)
Surface Mesh Maximum Size	0.01 (m)
Cell Volume Element	Polyhedral
Fill Type	Uniform, Smoothing Transition

#### 2.2.3. Governing Equations in CFD Analysis

The Navier-Stokes equation for a fully developed laminar fluid flow (Body water) with a constant density ( $\rho$ ) and dynamic viscosity ( $\mu$ ) was used in solving the CFD simulation.

$$\rho \frac{\partial u}{\partial t} - \mu \nabla^2 u + \rho(u. \nabla) u + \nabla p = F, \tag{1}$$

The variables of  $\rho$ , u, and  $\mu$  are density (kg/m³), velocity (m/s), and dynamic viscosity (kg/m.s).  $\nabla$  this is defined as the del operator, and p is defined as pressure (Pa). F is forces within the system [10].

## 2.2.4. Fluid Properties and Boundary Conditions

Fluid dynamics analyses are essential for understanding blood flow through porous micro-structures, as they determine the transport of nutrients and oxygen to cells and the flushing of toxic waste [20]. No stem cells were directly included in this study. It is assumed that the flow of material is Newtonian, and the presence of stem cells will not significantly affect fluid properties. However, the parameters chosen for this study are based on a simulated body fluid reported in [5], having a

temperature of 37 °C, a density of 1000 kg/m<sup>3</sup>, and a dynamic viscosity of 1.45E-3 Pa.s.

The boundary conditions of the CFD models are demonstrated in Figure 2. The inlet velocity value is 0.001 m/s [5]. In addition, the model and the wall have the no-slip condition applied to their surface structures. As for the pressure outlet, the gauge pressure is set to 0 Pa.

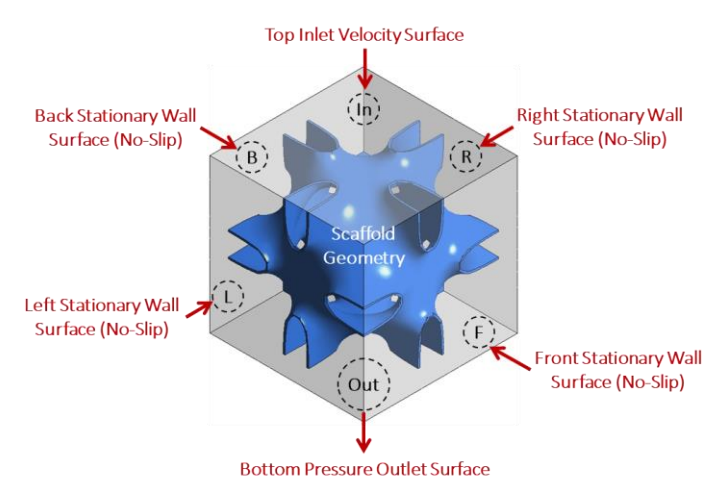


**Figure 2:** THE BOUNDARY CONDITIONS OF THE CFD MODELS. THE INLET VELOCITY IS SET AT 0.001 M/S, AND THE PRESSURE OUTLET IS AT 0 PA-G.

#### 2.2.5. Numerical Solutions

The method that was used for the scheme of the simulation is the coupled scheme. The coupled scheme has an improvement over a non-coupled or segregated approach. The coupled scheme has a robust and efficient single-phase implementation for steady-state flows. In addition, using the coupled scheme benefits when the mesh quality is poor or if significant time steps are used [19].

The method used for the Gradient is a Least squared Cell Based. If a mesh is a skewed and distorted structure, the accuracy of the least-squares gradient method is equivalent to that of a node-based gradient. In addition, this method is less expensive in computing than that of a node-based gradient. As for the momentum, a Second-order upwind scheme is used to solve the momentum equation. The Second-order upwind Scheme is less diffusive than that of its First-order counterpart.

Furthermore, for the pseudo-time method, a Global Time Step was applied. For it yields a specific explicit underrelaxation of the equation can be controlled for an update of the computed variables for each iteration [19].

## 2.2.6. Verification and Validation

Verification and validation of computational modeling are critical to ensure the accuracy of the analysis. The numerical solution will reflect the natural transportation phenomena of the bone scaffold fluid properties.

#### a. Validation

The published work of *Wang et al.* [5] was followed to validate the CFD models' accuracy. Their work focused on CFD analysis of a bone scaffold using Schwarz P design. The pressure and velocity values observed in this study are comparable to the results reported by Wang *et al.* Only minor differences can be observed where both results show favorable values and likeness to one another. The variation of the values can be due to our CFD model's dimensions as well as the flow domain's tolerance around the bone scaffolds. In addition, the same boundary conditions and fluid properties were used in this study.

#### b. Verification

The pressure and velocity boundary conditions were contrasted against the computational pressure and velocity results [21]. For all simulations, it was observed that the boundary conditions were satisfied, remaining unchanged at the set boundary values, with the inlet velocity being at 0.001 m/s and the pressure outlet gauge being at 0 Pa.

## 3. RESULTS AND DISCUSSION

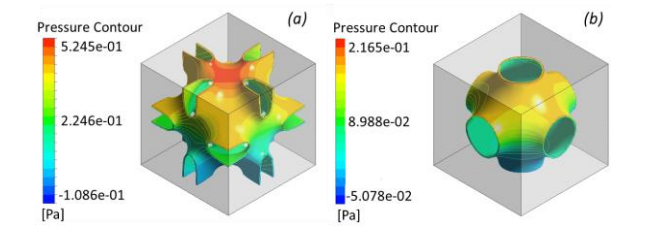
## 3.1. Internal Flow Simulation

## 3.1.1. Pressure Contours Analysis

The internal flow simulation results for the models' profile pressure are shown in Figure 3. The pressure within the model displays higher pressure at the inlet velocity and gradually dissipates the pressure at the outlet. It results in satisfying the boundary condition of the model requirements.

Thus, design (g) has the highest-pressure output, with design (a) following second to it. These models have a flatter surface area when compared to that of design (b), i.e., Schwarz P, which has a more curved geometry. The range of the pressure output is 8.64E-1 to 2.17E-1 Pa.

In addition, design (b) is the lowest pressure output of all 10 TPMS models within the analysis. The geometry of design (b) has a decrease in pressure along the sides of the curved portion of the model. This results in the side of the scaffold increasing velocity in those areas. Furthermore, designs (h), (i), and (j) have moderate pressure value output within the study; these geometries have a greater curved surface area than that of design (b). Therefore, it leads to the fluid passing through the model's pores to interact with the wall and cause a fraction on the surface, thus resulting in a pressure build-up.



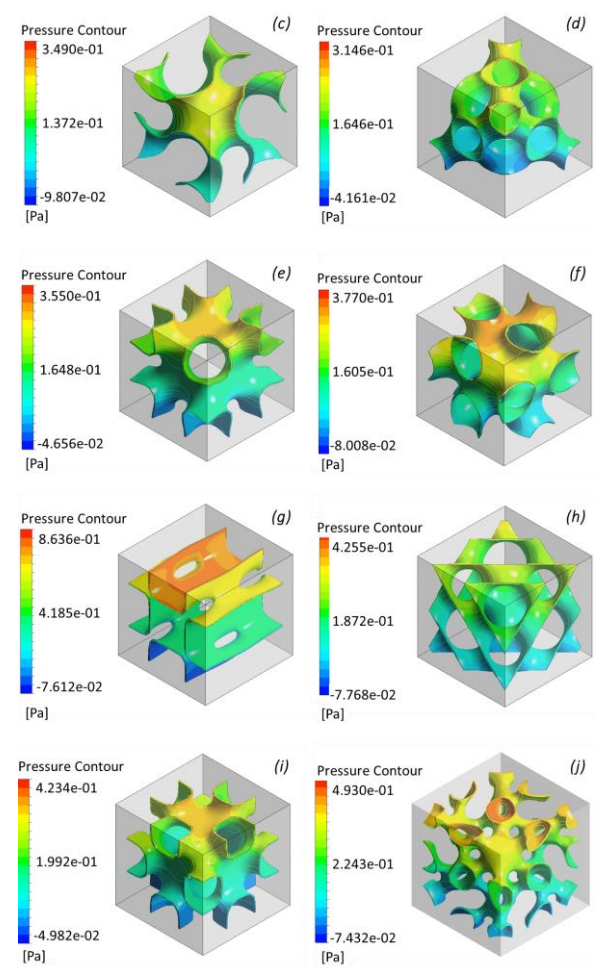


**Figure 3:** INTERNAL PRESSURE CONTOURS FOR ALL 10 TPMS DESIGNS.

## 3.1.2. Wall Shear Stress Analysis

A Wall Shear Stress (WSS) Analysis was performed on all 10 TPMS designs; WSS is regarding the forces of fluid interactions along the wall of the structure on the model. Furthermore, the model's boundary condition is no-slip, and the fluid flow is laminar for the fluid properties. Within Figure 4, the highest and lowest max ranges of the WSS can be seen at 3.64E-1 to 1.21E-1 Pa, respectively. Design (a) and (g) have the highest values of WSS. In addition, these models also demonstrated to have higher values of pressure as well.

Furthermore, the scaffold designs display a lower value gradient of WSS on curved segments on the models. Thus, these conditions of lower WSS values can promote bone proliferation for cell development. For average WSS values, 0.1 to 10 mPa must be around to induce healthy bone development. Thus, with the observation within Figure 4, the curved geometry can live within those desired conditions of lower WSS values that can be detailed with the channel and curved section of the geometry [9].

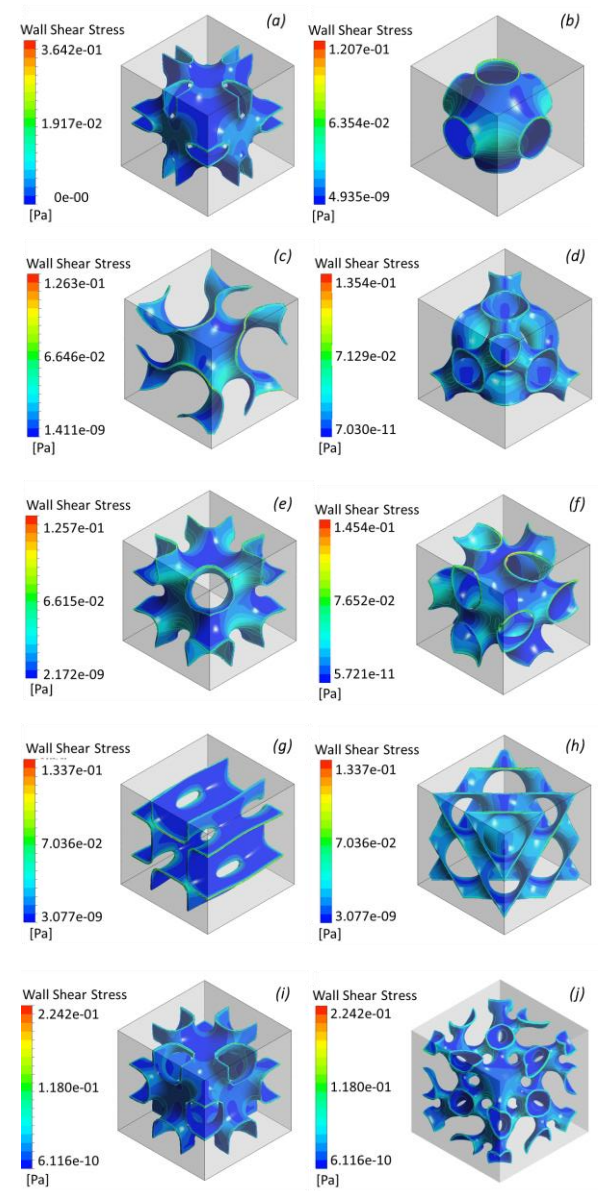


**Figure 4:** INTERNAL WALL SHEAR STRESS (WSS) CONTOURS FOR ALL 10 TPMS DESIGNS.

#### 3.1.3. Velocity Streamline Analysis

Within Figure 5, the velocity streamlines analysis shows an increase in velocity along the curved section of the geometry. The range of max velocity streamlines is 5.57E-03 to 3.54E-03 (m/s). Furthermore, the max velocity value of design (g) is 5.57E-03 (m/s), with design (d) having a max velocity of 4.55E-3 (m/s). Design (g), velocity can be seen slowing down at the flat segments of the structure due to the no-slip condition. The fluid flow passes into the narrow channels of the structure, resulting in an increase in velocity due to a decrease in cross-sectional area. As for design (d), the geometry consists of the structure mainly being developed into curved portions. Therefore, the velocity will increase within the narrow channels of the structure, resulting in a decrease in pressure within those

sections. Thus, WSS can have an effect resulting in biofluid interaction along the surface structure. That will allow for biodevelopment to take place.

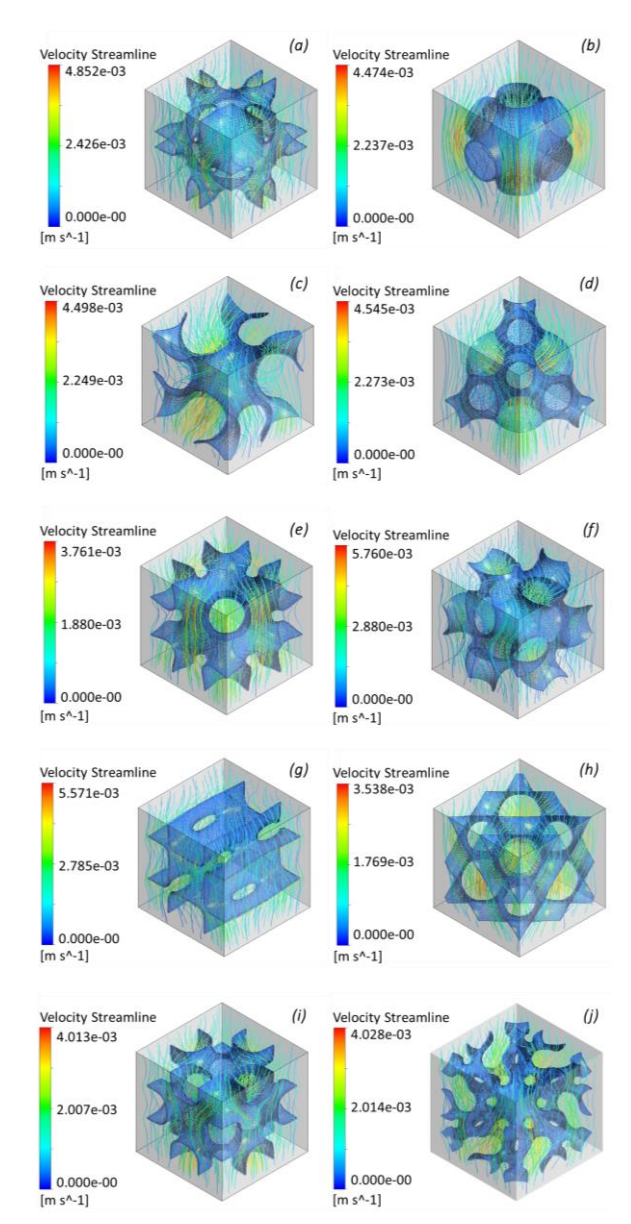


**Figure 5:** INTERNAL VELOCITY STREAMLINES FOR ALL 10 TPMS DESIGNS.

# 3.2. External Flow Simulation

## 3.2.1. Pressure Contour Analysis

The models' profile pressure of external flow simulation results can be seen in Figure 6. The pressure within the model displays higher pressure at the inlet velocity and gradually dissipates the pressure at the outlet. Thus, the results satisfy the boundary condition requirements. In addition, the maximum pressure value range is 9.14E-2, with the lowest being 4.0E-2 Pa.

Design (a) yields the highest-pressure output within the inlet section, which contains the area of the highest-pressure location.

In parallel to the internal flow, the flat surface area of the geometry in collaboration with the small pores creates a difficult flow path for the fluid to pass through. Thus, a cumulation of pressure is built up within the inlet portion of the fluid flow.

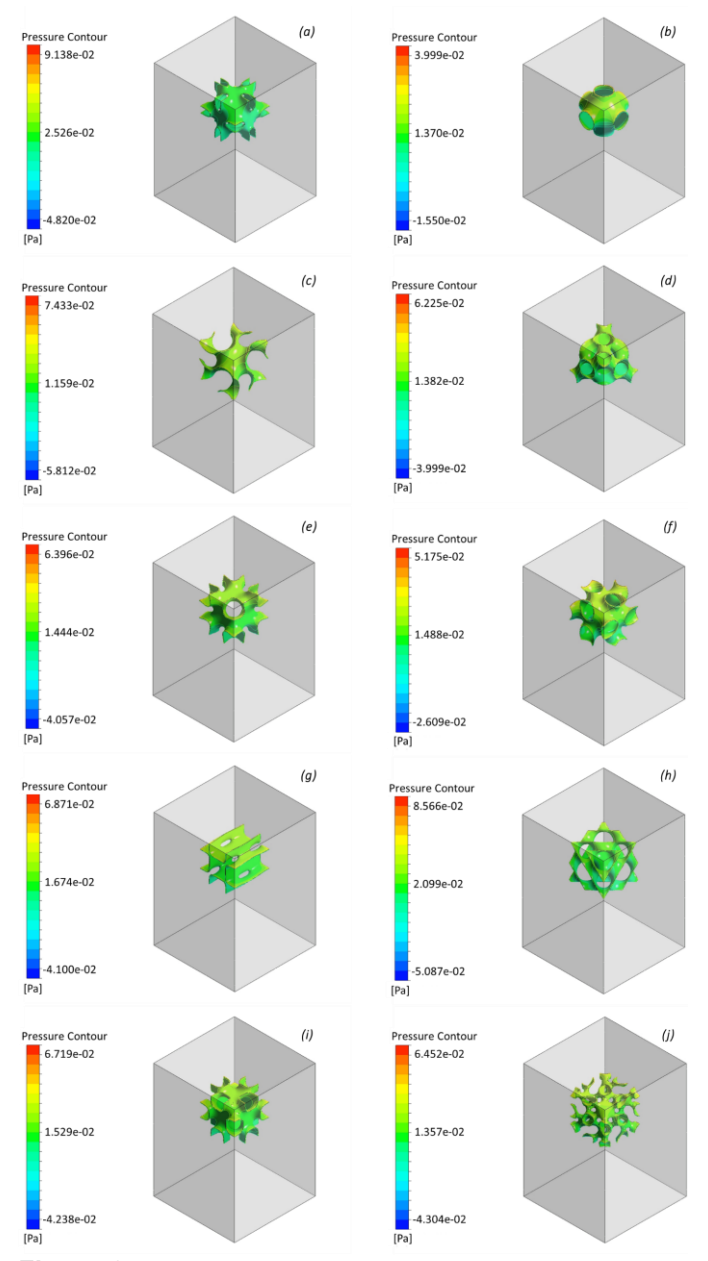


**Figure 6:** EXTERNAL PRESSURE CONTOURS FOR ALL 10 TPMS DESIGNS.

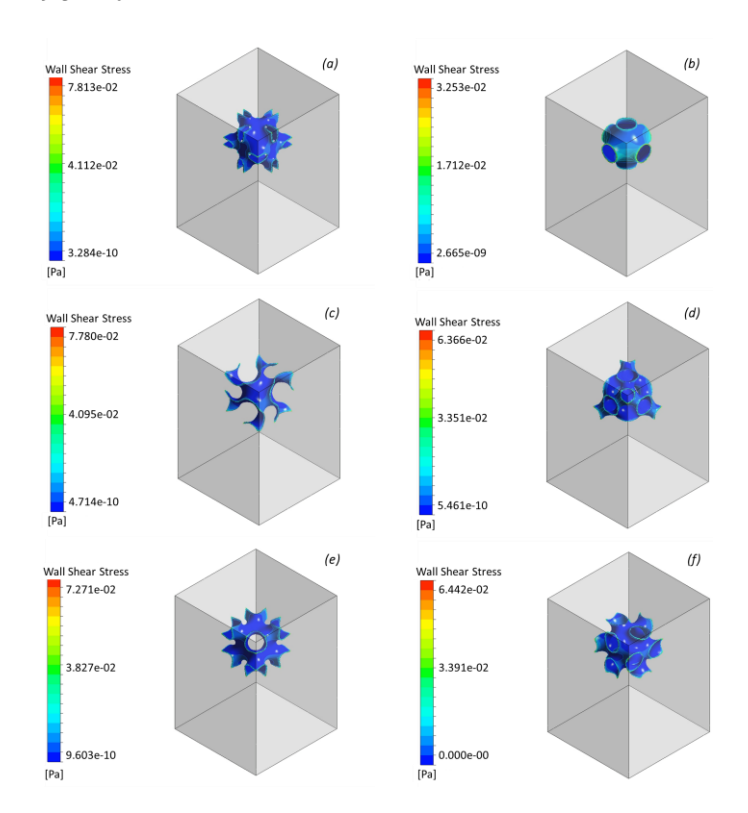
The design (b) produced the lowest pressure value output, much like it did within the internal flow. The geometry of design (b) has a decrease in pressure along the sides of the curved portion of the model, similar to the past result. In addition, the reduction in pressure can also be attributed to the dominant open pore at the inlet position, thus allowing the fluid flow to pass without difficulty.

Furthermore, design (h) yields a pressure output value of 8.57E-02. Unlike the internal flow counterpart, it yields an average pressure output of 4.26E-01. The increase in pressure can be attributed to the flow build-up within the scaffold along the inlet portion of the flow. Due to the complexity of the curvature, the flow is induced to interact along the structure's wall, slowing it down. This results in a model with a complex curvature structure capture the fluid, which will allow for biofluid to interact with the structure, resulting in the promotion of bone proliferation.

## 3.2.2. Wall Shear Stress Analysis

With the evaluation of the WSS Analysis on the external flow that can be seen in Figure 7, the highest to lowest max values of WSS are 9.32E-02 and 3.25E-02 Pa. Thus, this also satisfies the desired conditions in promoting bone proliferation cell development [9], where the WSS average needs to be around 0.1 and 10 mPa.

Furthermore, design (h) displays having the highest values WSS value within the external flow analysis due to the results of fluid interaction that accrues with complex curved structures. With design (b), the curvature is simple compared to design (h), where design (b) WSS value is 3.25E-02 Pa and design (h) shows 9.31E-02 Pa.



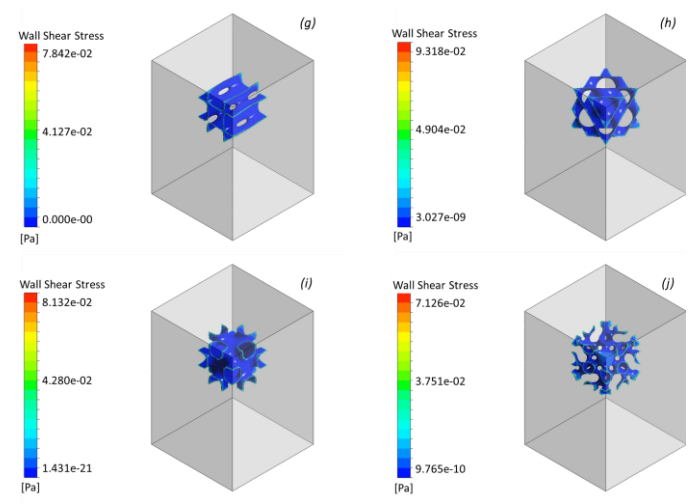
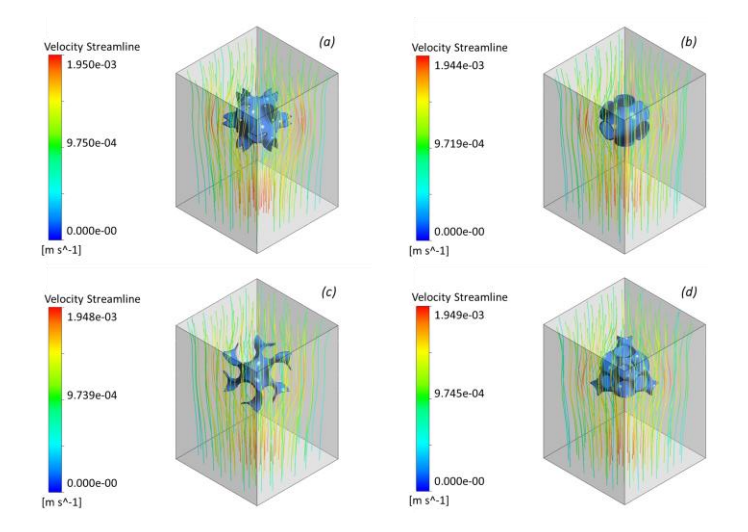


**Figure 7:** EXTERNAL WALL SHEAR STRESS (WSS) CONTOURS FOR ALL 10 TPMS DESIGNS.

## 3.2.3. Velocity Streamline Analysis

Within Figure 8, external velocity streamlines analysis shows the increase in velocity along the curved section of the geometry. The range of max velocity streamlines is 1.955E-03, and the lowest velocity is 0.00 (m/s).

Furthermore, the average max velocity is 1.942E-03 of all 10 TPMS designs. The velocity streamlines can be seen in increasing velocity as the fluid passes over the structure. In addition, the induction of a turbulent wake region development toward the end of the model is absent. This is due to the low-velocity initial conditions. Furthermore, when looking at designs like Schwarz G (design (c)), the depiction of turbulent motion can be seen along the internal curved sections of the scaffold. As the external velocity streamlines decrease within the inner channels of designs, this will lead to an increased pressure buildup as the fluid interacts with the model's walls. Furthermore, this will support the production of biofluid interaction and the development of bone structure.



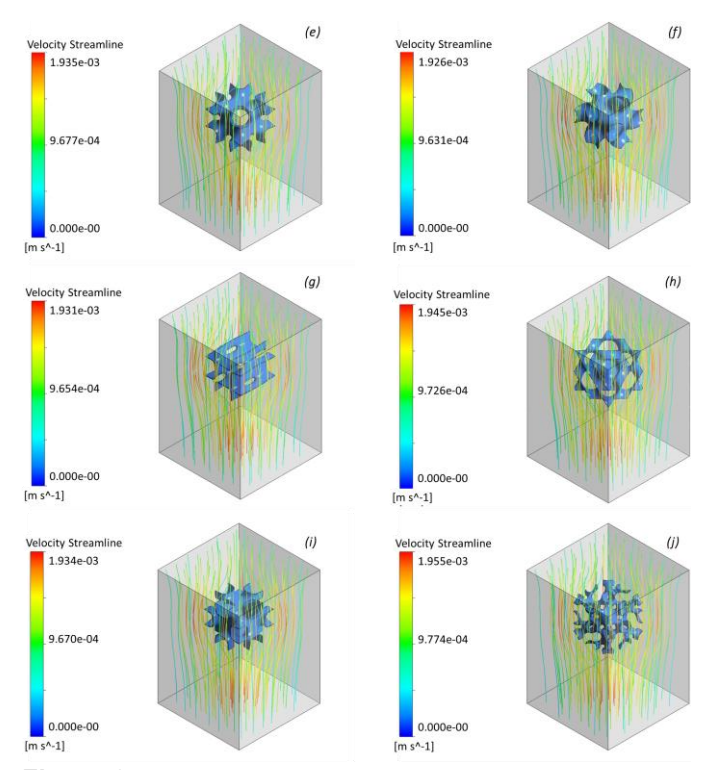


**Figure 8:** EXTERNAL VELOCITY STREAMLINES FOR ALL 10 TPMS DESIGNS.

# 3.3. Significance and Biological Implications of the Results

It is critical to understand the influence of WSS, pressure, and velocity and how they affect cell viability. WSS affects the differentiation ability of cells to renew tissues and aids in forming a single cell layer that lines all blood vessels and regulates exchanges between the bloodstream and the surrounding tissues [20]. In addition, pressure affects cell viability and survival within the hemodynamics of the blood shear flow, potentially acting as a mechanical stimulus on cells; pressure also affects the biological activity of scaffolds and influences scaffold-cell interactions [20]. As for the importance of velocity, streamlines show how the bloodstream would pass through the scaffolds' architecture. Furthermore, velocity streamlines reveal how the bloodstream passes through the scaffolds' architecture in addition to showing turbulent motion that can accrue within the scaffold channels. Besides, capturing changes in velocity leads to implications in terms of cell-wall interactions, which give insights into where cell attachment and adhesion may occur.

## 3.4. Identification of Optimal Designs

It is essential to note that the lowest pressure and WSS results have the most potential for stem cell viability and allow osteoblast to occur. Figure 9 illustrates a bar graph of maximum pressure (a) and WSS (b) for all TPMS scaffold designs. It was observed that *Schwarz P* would have a favorable performance, having the lowest level of pressure as well as WSS, relatively. Therefore, Schwarz P is the optimal design when considering the

interaction of fluid properties. Furthermore, all Schwarz designs similarly showed favorable outcomes, having a low level of pressure and WSS. In addition, Schoen I-WP turned out to be a viable option as it comes as the second design in terms of WSS.

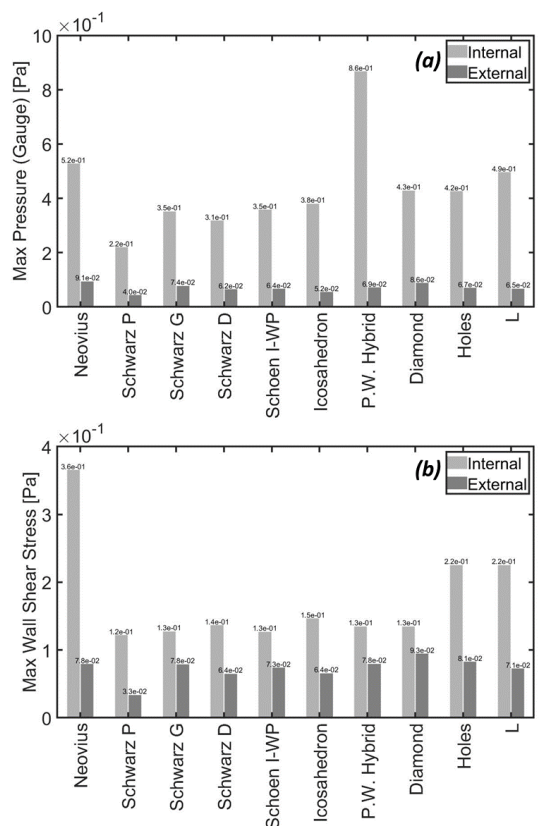


**Figure 9:** BAR GRAPHS COMPARING MAXIMUM PRESSURE AND WALL SHEAR STRESS WITH RESPECT TO DESIGN 1-10.

Please note that in terms of geometrical factors, porosity, shape, dimensions, as well as fluid-material interactions, additively manufactured scaffolds are expected to yield results similar to those reported in this study. However, material properties, composition, and manufacturing-related properties (such as surface roughness) will play a significant role in the fluid transport through the scaffolds, which may considerably affect the reported values of pressure, WSS, and velocity.

## 4. CONCLUSIONS AND FUTURE WORK

### 4.1. Conclusions

In conclusion, the overall objective of this work is to fabricate a CFD model from Rhinoceros 3D software to identify the significant mechanisms within internal and external material transport for porous bone scaffolds using ANSYS software. Furthermore, the TPMS scaffold designs of 10 internal-flow and 10 external-flow CFD models observed material transport fluid characteristics of flow velocity, flow pressure, and wall shear stress, respectively.

## a. Internal Flow:

The pressure flow analysis for internal flow findings shows that design 7 P.W. Hybrid has the highest-pressure output at 8.636E-01 Pa; this is a result of the architecture of the design being flatter than that of the more complex curved geometry. For instance, design models 2, 3, and 4 (Schwarz P, Schwarz G, and Schwarz D) are shown to have lower pressure due to the channels of the design allowing for more effortless fluid flow within the geometry, which can be seen within the internal flow velocity characteristics were the velocity streamline show an increase in the rate at a section where the design yields more complex curvature and more narrow channel for the fluid to travel. Furthermore, the WSS analysis of max ranges delivered at 3.64E-1 to 1.21E-1 Pa, Design 1: Neovius, and Design 7: P.W. Hybrid have the highest values of WSS in addition, and these scaffold designs also demonstrated to have higher values of pressure as well. In addition, average WSS values of 0.1 to 10 mPa induce bone development within a curved section and channels of the scaffolds that yield lower WSS values.

## b. External Flow:

The pressure flow analysis for external flow showed that the maximum pressure value range is 9.14E-2 to 4.00E-2 Pa, respectively. Thus, design 1: Neovius yields the highest-pressure output along the inlet section; this is due to the flat surface area of the geometry in collaboration with the small pores. Resulting in a difficult flow path; thus, a cumulation of pressure is built up within the inlet portion of the fluid flow. The geometry of design 2: Schwarz P has a decrease in pressure along the sides of the curved portion; the reduction in pressure can also be attributed to the dominant open pore at the inlet position, allowing the fluid flow to pass without difficulty. Design 8: Diamond has an increase in pressure at a value of 8.57E-02 Pa; this can be attributed to the flow build-up within the structure along the inlet portion of the flow. Due to the scaffold design having complex curved channels capturing the fluid, which can be seen within the velocity streamline section of the results aiding in this understanding of fluid dynamics analysis. In addition, the max values of WSS are 9.32E-02 and 3.25E-02 Pa from highest to lowest. Thus, within the scaffold design section where the channels and curved portion of the geometry yield lower values, the desired conditions for promoting bone proliferation cell development can be produced.

Furthermore, design 8: Diamond displays have the highest values WSS value within the external flow analysis due to the results of fluid interaction that accrues with complex curved structures. External velocity streamlines analysis shows the range of max velocity streamlines is 1.955E-03, and the lowest velocity is 0.00 (m/s), where the average max velocity is 1.942E-03. The analysis shows an increase in rate as the fluid passes over the structure. In addition, the induction of a turbulent wake region development toward the end of the model is absent. Also, designs with curved geometries, like that of Schwarz G, can be seen to have turbulent motion within the internal channels of the scaffold. Furthermore, external velocity streamlines decrease within the inner channels of designs, leading to an increased

pressure build-up as the fluid interacts with the model's walls, thus aiding in the production of biofluid interaction and the development of bone structure.

#### 4.2. Future Work

The understanding that was brought by the CFD analysis of the internal and external flow has aided in understanding the dynamics of fluid interaction of TPMS scaffold designs. Yet there are still gaps of understanding within this area, like how fluid interaction will affect the strength of the scaffold. In addition, how does smoothness affect the scaffold performance in developing quality bone proliferation? Lastly, an experimental test is done to show actual fluid dynamics within the porous scaffold cubes.

The designed scaffolds can be fabricated for bone tissue engineering using, for example, fused deposition modeling (FDM) and selective laser sintering (SLS) additive manufacturing. It is worth mentioning that four of the ten designs have been fabricated by the authors, as detailed in [4], where scaffolds with satisfactory mechanical strength, rigidity, and stability were obtained for bone regeneration. The rest of the designs will be characterized as part of the authors' future work.

## **ACKNOWLEDGMENTS**

Dr. Salary would like to acknowledge the National Aeronautics and Space Administration (NASA) for supporting this work under grant # 80NSSC22M0249 (EPSCoR-R3). In addition, Dr. Salary would like to thank the National Science Foundation (NSF) for funding this work under award # 0IA-2327460; investigation of material transport in advanced manufacturing using computational fluid dynamics models was one of the main aspects of the award.

## **REFERENCE**

- [1] Lawrence, L. M., Salary, R., Miller, V., Valluri, A., Denning, K. L., Case-Perry, S., Abdelgaber, K., Smith, S., Claudio, P. P., and Day, J. B., 2023, "Osteoregenerative Potential of 3D-Printed Poly ε-Caprolactone Tissue Scaffolds In Vitro Using Minimally Manipulative Expansion of Primary Human Bone Marrow Stem Cells," International Journal of Molecular Sciences, 24(5), p. 4940, DOI: 10.3390/ijms24054940.
- [2] Abdelgaber, Y., Klemstine, C., and Salary, R., 2023, "A Novel, Image-Based Method for Characterization of the Porosity of Additively Manufactured Bone Scaffolds With Complex Microstructures," Journal of Manufacturing Science and Engineering, 145(4), p. 041008, DOI: 10.1115/1.4056434.
- [3] Yu, M., Yeow, Y. J., Lawrence, L., Claudio, P. P., Day, J. B., and Salary, R., 2021, "Characterization of the Functional Properties of PCL Bone Scaffolds Fabricated Using Pneumatic Microextrusion" Journal of Microand Nano-Manufacturing, JMNM-20-1074, DOI: 10.1115/1.4051631.
- [4] Coburn, B., Joyce, R., and Salary, R., "Investigation of the Influence of Nylon-6 vs. Nylon-66 on the Mechanical Performance of Composite Bone Tissue Scaffolds," Proc. ASME International Mechanical Engineering Congress and Exposition, American Society of Mechanical Engineers, p. V003T003A087, DOI: 10.1115/IMECE2023-110405.
- [5] Wang, S., Liu, L., Zhou, X., Zhu, L., and Hao, Y., 2020, "The Design of Ti6Al4V Primitive Surface Structure with Symmetrical Gradient of Pore Size in Biomimetic Bone Scaffold," Materials & Design, 193, p. 108830, DOI: 10.1016/j.matdes.2020.108830.
- [6] Li, Z., Chen, Z., Chen, X., and Zhao, R., 2022, "Effect of Surface Curvature on the Mechanical and Mass-Transport Properties of Additively Manufactured Tissue Scaffolds with Minimal Surfaces," ACS Biomaterials

- Science & Engineering, 8(4), pp. 1623-1643, DOI: 10.1021/acsbiomaterials.1c01438.
- [7] Ma, S., Tang, Q., Han, X., Feng, Q., Song, J., Setchi, R., Liu, Y., Liu, Y., Goulas, A., and Engstrøm, D. S., 2020, "Manufacturability, Mechanical Properties, Mass-Transport Properties and Biocompatibility of Triply Periodic Minimal Surface (TPMS) Porous Scaffolds Fabricated by Selective Laser Melting," Materials & Design, 195, p. 109034, DOI: 10.1016/j.matdes.2020.109034.
- [8] Kim, D., Peng, C., Tran, J., and Philip, J., "An Experimental Study of Pressure Drop and Fluid Flow in Triply Periodic Minimal Surface (TPMS) Scaffolds," Proc. 12th International Symposium on Turbulence and Shear Flow Phenomena (TSFP12), Osaka, Japan, July 19–22, 2022, ReH, pp. 1-4. DOI: N/A.
- [9] Pires, T. H., Dunlop, J. W., Castro, A. P., and Fernandes, P. R., 2022, "Wall Shear Stress Analysis and Optimization in Tissue Engineering TPMS Scaffolds," Materials, 15(20), p. 7375, DOI: 10.3390/ma15207375.
- [10] Ali, D., Ozalp, M., Blanquer, S. B., and Onel, S., 2020, "Permeability and Fluid Flow-Induced Wall Shear Stress in Bone Scaffolds with TPMS and Lattice Architectures: A CFD Analysis," European Journal of Mechanics-B/Fluids, 79, pp. 376-385, DOI: 10.1016/j.euromechflu.2019.09.015.
- [11] Pires, T., Dunlop, J. W., Fernandes, P. R., and Castro, A. P., 2022, "Challenges in Computational Fluid Dynamics Applications for Bone Tissue Engineering," Proceedings of the Royal Society A, 478(2257), p. 20210607, DOI: 10.1098/rspa.2021.0607.
- [12] Kumar, J., Nirala, N. s., Singh, N. K., Gupta, N., Dwivedi, Y. D., Verma, R., Rai, S. K., and Gupta, M., 2023, "Design, Development and Fluidic Behavior Analysis of Triply Periodic Minimal Surface (TPMS) Based Scaffolds for Bone-Aplications," International Journal on Interactive Design and Manufacturing (IJIDeM), pp. 1-11, DOI: 10.1007/s12008-023-01441-2.
- [13] Deng, F., Liu, L., Li, Z., and Liu, J., 2021, "3D Printed Ti6Al4V Bone Scaffolds with Different Pore Structure Effects on Bone Ingrowth," Journal of biological engineering, 15, pp. 1-13, DOI: 10.1186/s13036-021-00255-8.
- [14] Daver, A., "Scaffolds for Bone Using Inclined Schwarz TPMS; Design and Finite Element Analysis," Proc. International Science and Art Research Congress (ISARC), Istanbul, Turkey, 24-25 December 2022., p. 5, DOI: N/A
- [15] Singh, S., Yadav, S. K., Meena, V. K., Vashisth, P., and Kalyanasundaram, D., 2023, "Orthopedic Scaffolds: Evaluation of Structural Strength and Permeability of Fluid Flow via an Open Cell Neovius Structure for Bone Tissue Engineering," ACS Biomaterials Science & Engineering, 9(10), pp. 5900-5911, DOI: 10.1021/acsbiomaterials.3c00436.
- [16] Guerreiro, R., Pires, T., Guedes, J. M., Fernandes, P. R., and Castro, A. P., 2020, "On the Tortuosity of TPMS Scaffolds for Tissue Engineering," Symmetry, 12(4), p. 596, DOI: 10.3390/sym12040596.
- [17] Li, Z., Chen, Z., Chen, X., and Zhao, R., 2023, "Design and Evaluation of TPMS-Inspired 3D-Printed Scaffolds for Bone Tissue Engineering: Enabling Tailored Mechanical and Mass Transport Properties," Composite Structures, p. 117638, DOI: 10.1016/j.compstruct.2023.117638.
- [18] Salary, R., 2022, "Perspective Chapter: Advanced Manufacturing for Bone Tissue Engineering and Regenerative Medicine," Advanced Additive Manufacturing, I. V. Shishkovsky, ed., IntechOpen, London, UK, p. 59, DOI: 10.5772/intechopen.102563.
- [19] ANSYS-Fluent, 2015, "16.2 Theory Guide," ANSYS Inc., Canonsburg, PA.
- [20] Omar, A. M., Hassan, M. H., Daskalakis, E., Ates, G., Bright, C. J., Xu, Z., Powell, E. J., Mirihanage, W., and Bartolo, P. J., 2022, "Geometry-Based Computational Fluid Dynamic Model for Predicting the Biological Behavior of Bone Tissue Engineering Scaffolds," Journal of Functional Biomaterials, 13(3), p. 104, DOI: 10.3390/jfb13030104.
- [21] Salary, R., Lombardi, J. P., Weerawarne, D. L., Rao, P., and Poliks, M. D., 2021, "A Computational Fluid Dynamics Investigation of Pneumatic Atomization, Aerosol Transport, and Deposition in Aerosol Jet Printing Process," Journal of Micro-and Nano-Manufacturing, 9(1), p. 010903, DOI: 10.1115/1.4049958.